Journal of Hydraulic Structures
J. Hydraul. Struct., 2021; 7(1):
DOI:

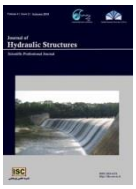

OPEN ACCESS

Investigation of Deepwater horizon oil spill movement in the Gulf of Mexico

Hamid Goharnejad [1]
Will Perrie [2]

Abstract

In this paper, the performance of the MIKE21 numerical model in modeling the dispersion and transport of spilt oil related to the Deep-Water Horizon oil platform disaster in the northern part of the Gulf of Mexico is studied. Our model predicts the distribution and movement of spilt oil based on the wind-waves, current flows and vorticities taking into account evaporation, emulsion, and absorption. In this research, two types of large scale and local scale models are considered. The radiation stress of the waves, the water level and the flow speed in the Gulf are modeled using a large-scale model. After calibration and verification, the large-scale model is used to extract the boundary conditions for the local scale model and the dispersion and transport of the spilt oil is done in the local model. The accuracy of the numerical simulation using MIKE21 are confirmed by comparisons to observed satellite images. Results showed that the length of the oil spill reached 55 kilometers and covered an area of 2,800 Km2 by April 25. After two weeks, the oil spill had apparently divided into two slicks, each with an area of about 2420 and 960 Km2, respectively. Eventually, by May 28, the slick area appeared to reach over 48,400 Km2 which much of the oil evaporated because it was lightweight oil. Meanwhile, the Deep-Water Horizon oil spill occurred in spring and summer seasons; we also consider possible results assuming that the spill occurred at other times, such as autumn or winter.

Keywords: Deep water Horizon oil spill, satellite images of spilt oil, spectral wave model, flow model, vorticities, Gulf of Mexico.

Received: 08 March 2021; Accepted: 02 June 2021

1. Introduction

An oil spill occurs with the release of liquid petroleum hydrocarbons into the environment, for example the marine ecosystem, resulting in pollution or contamination. Dispersion of oil pollutants into aqueous environments involves dispersion and transport, evaporation, suspension of hydrocarbons in gas particles, emulsion of oil particles, oil-beach and oil-ice interactions, and precipitation of oil particles (Raoufi et al, [1]; Asadi et al, [2]).

[1] Fisheries and Oceans Canada, Bedford Institute of Oceanography, Dartmouth, Nova Scotia B2Y 4A2, Canada **(Corresponding Author)**
[2] Fisheries and Oceans Canada, Bedford Institute of Oceanography, Dartmouth, Nova Scotia B2Y 4A2, Canada

Subsequent stages include photo-oxidation and biochemical decomposition (ASCE Task Committee, [3]). When oil is released into the water, it creates an oil layer. Regardless of what causes the release of oil pollution, the two general mechanisms of dispersion and transport can be characterized as being more effective than other factors in the distribution of oil pollutants. Both mechanisms contribute to the spatial dispersion of pollutants through sea currents, winds and waves. When an oil spill in the sea is affected by wind and waves, pushed across the water, it will experience reduced thickness and increased evaporation rates and the oil viscosity gradually increases (Javid, [4]).

Thus, the cleanup and recovery of spilt oil in the marine environments is difficult and depends upon many factors. Numerical modeling is one of the methods that can help to predict the wave parameters (Armanfar et al, [5]; Goharnejad, and Eghbali, [6]) and movement of an oil spill and thus assist the associated mitigation actions.

The dramatic rise in maritime hazards has led researchers to develop a variety of sophisticated, diverse models to forecast the dispersal and transport of spilt oil. Fay [7,8], Stolzenbach [9] and Lehr [10] provided formulae for the dispersal of oil slicks, where they considered a controlled condition, such as given volume of oil discharge and calm sea. Elliott [11] simulated the spread of spilt oil spill in response to winds and waves, considering lateral and vertical shear-induced diffusion. Weber [12] and Jenkins [13] developed complex, accurate models to study the movement of oil spills in deep waters, taking into account the effects of winds, currents, waves, and their interactions with each other in the ocean surface layer. The oil spill fate and transport model, OILPOL, was also presented by Al-Rabeh [14] and has been applied to compute the distributions of surface and subsurface oil and analyze the fate of spilt oil. A model for the formation process of water-in-oil emulsions was presented by Fingas and Fieldhouse [15]. With the increasing importance and extent of oil pollution incidents in recent years, more studies have also been conducted. Owens et al, [16] examined the sustainability and variability of stranded oil on coarse-sediment beaches. Marianoa et al, [17] used prediction models to evaluate the fate of the two small oil spills in the pollutant complex resulting from the Deepwater Horizon (DWH) disaster in the Gulf of Mexico.

North et al, [18] simulated the oil droplet dispersal from DWH using a Lagrangian approach. This methodology used a multi-stage analytical model along with the SABGOM hydrodynamic model to simulate the motion of oil spills. The hydrodynamic model of SABGOM is used as input to a Lagrangian transport model (Zhang et al, [19]).

Marques et al, [20] conducted a numerical study using coupled models to investigate the Tramandaí beach oil spill. The three-dimensional hydrodynamic model, TELEMAC3D, and the ECOS model were used. Results show that the winds and currents were the major physical forces controlling the oil behavior and the final destination of the oil trajectory. Moreover, the final oil mass balance calculation indicates that approximately 15% of the oil mass was lost because of evaporation.

French-McCay et al, [21] studied trajectory and fate modeling of the oil released during the Deepwater Horizon blowout for April to September of 2010 using a variety of input data sets to determine the inputs leading to the best agreement with observations and to evaluate their reliability for quantifying exposure of marine resources to floating and subsurface oil.

An oil spill occurred off Port Lach Huyen in the northeast region of Vietnam in 2011, due to a ship collision. Tri et al, [21] simulated the oil spill transport using five scenarios, with the MIKE 21 SA model. The results helped to elucidate eco-sensitive regions for preparedness and planning of suitable response strategies in the event of future spill incidents.

Pisano et al, [23] provided a criterion to identify positive and negative oil-water contrast

regions in observations using MODIS near-infrared sun glittered radiance imagery. Results showed that application of threshold criteria is able to isolate the spills and that the spills of the validation dataset are successfully detected.

The Deepwater Horizon oil spill disaster occurred on April 20, 2010. Oil spill detection using SAR images in the Gulf of Mexico was studied by Wan and Cheng [24]. The results show that in the early stage of this accident, the shapes of oil slicks mainly appear as patches. As time increases, the tendency is for the appearance of the increasing prevalence of oil slicks appearing as stripes. Oil slick shapes and positions are affected by winds, ocean currents and related environmental factors. During the mid- and later periods of the Deepwater disaster, a portion of the spilt oil was deposited on the coasts of Louisiana, Alabama and Florida. In the early days of the oil spill, the size of the oil slicks tended to increase, reaching a peak in June. After July, the areas contaminated by the oil slicks began to decrease.

Caruso et al, [25] used Synthetic Aperture Radar (SAR) images from satellites to study the exploration, extraction, and transportation of the oil spills and slicks in the Gulf of Mexico. They showed that SAR can be used to direct response activities and optimize available resources for the DWH oil spill. Also, for the DWH oil spill, Sun et al, [26] used fine spatial resolution hyperspectral AVIRIS data, and evaluated slick lengths, widths and length/width ratios to determine oil slick morphology for different thickness classes. Khade et al, [27], studied the potential of ocean ensemble forecasting in the Gulf of Mexico and showed that this method has enormous potential benefits for the prediction of oil spill pathways.

Methods of oil detection in response to the DWH oil spill were also discussed by White et al, [28]. They believed that the oil detection technologies employed varied in sensitivity, selectivity, strategy, cost, usability, expertise of user, and reliability. Innovative technologies can produce new information relevant to spill detection, including chemical characterization, dispersant effectiveness, and the detection limits of various methodologies. The potential for environmental disturbances such as Hurricane Katrina in 2005 to interact a DWH-type oil spill was evaluated by Deis et al, [29] by calculating marsh shoreline retreat across both events. Although they could not detect a post-spill increase in marsh shoreline erosion, they concluded that Hurricane Katrina had reset the baseline for erosion.

In order to identify the spill's extent, Garcia-Pineda et al, [30] carried out analysis of SAR imagery during the DWH event, using a neural network approach, the Texture Classifier Neural Network Algorithm (TCNNA). Thus, they developed an oil emulsion detection algorithm using TCNNA outputs to enhance the contrast of pixels within the oil slick in order to identify SAR image signatures that may correspond to regions of thick, emulsified oil.

Oil spills in the northern Adriatic Sea were simulated by Loncar et al, [31] using MIKE model. They used a three-dimensional model for oil spill dispersion and transport that considered geopotential height, water temperature and salinity as ocean forcing fields. The modelling results of the physical oceanography parameters were validated by measurements from the 'Adriatic Sea Monitoring Program' at a series of current meter and CTD stations.

Badri and Faqhihi fard [32] also made numerical simulations of spilt oil based on an optimization of the turbulence flow pattern, including wind and tide effects, using MIKE21 in the Persian Gulf. In order to validate the model, they compared the flow and wave pattern results with data from current meters and buoys collected in 2008 and 2012.

Wave parameters are generally taken from *in situ* observations (buoys, tide gauges, ships), satellite altimeter observations or wave models. Wave regimes in Gulf of Mexico were studied by Appendini et al, [33]. They described wave climate and variability in the Gulf of Mexico based on a 30-yr wave hindcast. Their results show that the *mean* wave climate is mainly

modulated by winter cold fronts (Norte) in the Gulf of Mexico, whereas the *extreme* wave climate is dominated by both hurricanes and the Norte. Extreme wave heights in the Gulf of Mexico have increased at a rate of 0.07–0.08 m per year in September/ October because of increased cyclone intensity over the last decade. However, there is no significant trend with respect to the annual statistics for extreme events. Meanwhile, an integrated marine environment nowcast/forecast system including three models was introduced by Xue et al, [34]: WRF for ocean weather, SWAN for surface waves, and ROMS for ocean circulation for the South Atlantic Bight and Gulf of Mexico (SABGOM). Their results showed that the SABGOM system exhibits a reliable capability for providing valuable forecasts. Huang et al, [35] used SWAN wave model to consider the effects of wind input parameterizations on wave estimations under hurricane conditions in the Gulf of Mexico. The results show that based on the default wind input settings for hurricane cases, SWAN results are reliable for areas shallower than the shelf shoulder (20–30 m) region regardless of the model's tendency to overestimate SWH in deep waters.

In this paper, we study the oil spill dispersion and transport in the Gulf of Mexico related to the DWH disaster which occurred on April 20, 2010. Wind, wave and current flow regimes in the study area during the oil spill accident are extracted from the model system and the results are compared with satellite images. As a novelty, estimates are also constructed for the oil spill patterns assuming that the oil spill accident had happened in other seasons.

2. Study Area

The Gulf of Mexico is both a regional ocean basin and a marginal sea of the North Atlantic Ocean, largely surrounded by the North American continent. It is bounded on the northeast, north and northwest by the Gulf Coast of the United States, on the southwest and south by Mexico, and on the southeast by Cuba. The Gulf is connected to the Atlantic via Florida Strait between the United States and Cuba and by the Caribbean Sea between Mexico and Cuba (Figure 1). Due to considerable fossil fuel energy sources and its geopolitical position, this oval-shaped body of water plays an important role in North America's economics and political developments (Huerta, and D.L. Harry, [36]). The Gulf of Mexico covers about 1.6 million square kilometers and contains a volume of 2.5 million km^3 with an approximate width of 1500 km.

On April 20, 2010, the Deepwater Horizon (DWH) oil platform exploded and later sank in the Mississippi Canyon about 64 km off the Louisiana coast. The resulting oil slick quickly expanded to cover hundreds of square miles of ocean, posing a serious threat to marine life and adjacent coastal wetlands, and to the livelihoods of Gulf Coast shrimpers and fishermen. As of August 2, 2010, the spilt oil was initially estimated as 62,000 barrels daily, which later lessened to 53,000 barrels per day, with a total oil spill of 4.9 million barrels over 87 days (McNutt et al, [37]). The crude spilt oil was a complex mixture of hydrocarbons and other compounds with a relative density of about 0.85 grams per cubic meter which is lighter than sea water, with density 1.2 gr/cm^3 (Deep water Horizon MC 252 Response Unified Area Command, [38]). From the first appearance of the spilt oil in the Gulf on April 22, 2010, the spill area quickly expanded to 17725 square kilometers by May 17, 2010, 25 days later (Labson, [39]).

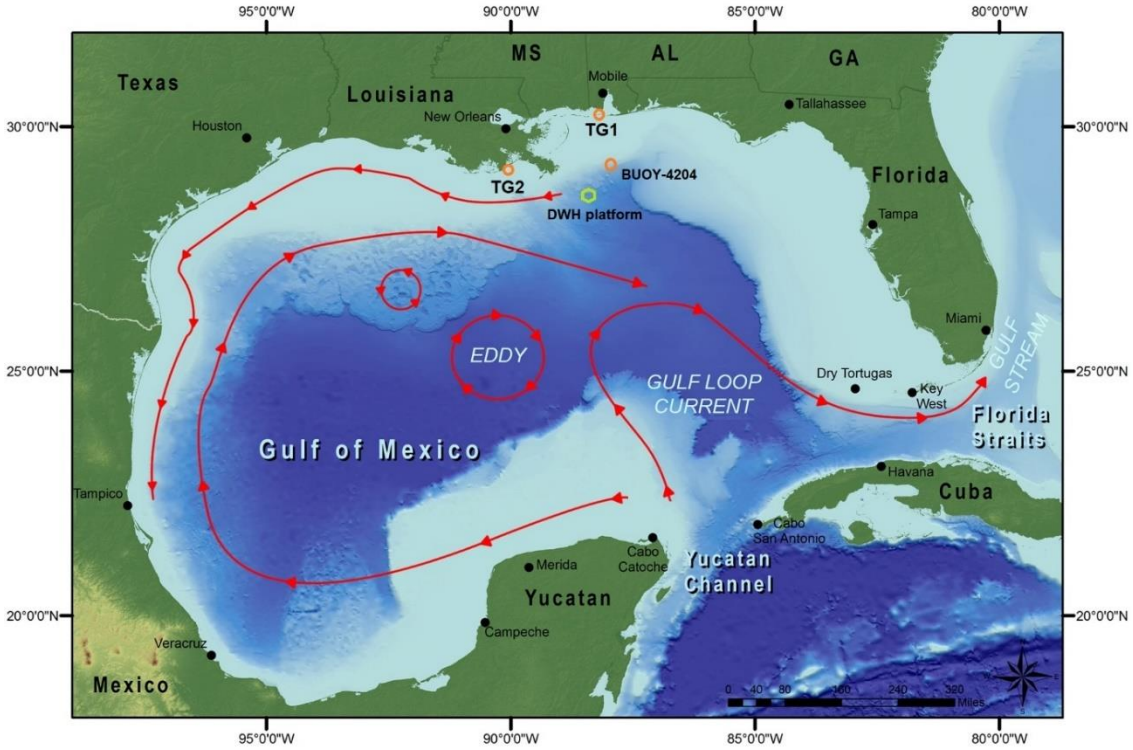

Figure 1. Geographic location of the Gulf of Mexico, the buoys, and the DWH platform.

3. Methodology and data collection

3.1. Hydrodynamic module

The MIKE numerical model was used to model both the flow and the waves spectra. MIKE is developed by the Danish Hydraulic Institute (DHI). The flow model simulates currents in a single-layer fluid (vertically homogeneous). Outputs of the flow model are used as inputs for a number of other MIKE modules, such as the oil spill module. The model simulates unsteady flows based on changes in density, depth, and external forces such as atmospheric forces, tidal forces and flow.

For Newtonian fluid flow, we used the mass continuity equation (Equation 1), and the momentum equation (Equations 2-4), for the salinity continuity and temperature, and the ratio of the density to salinity, temperature and pressure. These equations take into account the effects of turbulence and density changes with the salinity continuity and temperature relations. The turbulence model used in the present study is the well-known eddy viscosity turbulence model formulation by Smagorinsky.

$$\frac{\partial u}{\partial x}+\frac{\partial v}{\partial y}+\frac{\partial w}{\partial z}=0 \tag{1}$$

$$\frac{\partial u}{\partial t}+\mathrm{u}\frac{\partial u}{\partial x}+\mathrm{v}\frac{\partial u}{\partial y}+\mathrm{w}\frac{\partial u}{\partial z}=fv-\frac{1}{\rho_0}\frac{\partial P}{\partial x}+2\frac{\partial}{\partial x}\left(\mathrm{v_x}\frac{\partial \mathrm{u}}{\partial \mathrm{x}}\right)+\frac{\partial}{\partial y}\left(\mathrm{v_y}\left(\frac{\partial \mathrm{u}}{\partial \mathrm{y}}+\frac{\partial \mathrm{v}}{\partial \mathrm{x}}\right)\right)+\frac{\partial}{\partial z}\left(v_z\left(\frac{\partial u}{\partial z}+\frac{\partial w}{\partial x}\right)\right) \tag{2}$$

$$\frac{\partial v}{\partial t}+\mathrm{u}\frac{\partial v}{\partial x}+\mathrm{v}\frac{\partial v}{\partial y}+\mathrm{w}\frac{\partial v}{\partial z}=-fu-\frac{1}{\rho_0}\frac{\partial P}{\partial y}+\frac{\partial}{\partial x}\left(\mathrm{v_x}\left(\frac{\partial \mathrm{v}}{\partial \mathrm{x}}+\frac{\partial \mathrm{u}}{\partial \mathrm{y}}\right)\right)+2\frac{\partial}{\partial y}\left(\mathrm{v_y}\frac{\partial \mathrm{v}}{\partial \mathrm{y}}\right)+\frac{\partial}{\partial z}\left(v_z\left(\frac{\partial v}{\partial z}+\frac{\partial w}{\partial y}\right)\right) \tag{3}$$

$$\frac{\partial w}{\partial t} + \mathrm{u}\frac{\partial w}{\partial x} + \mathrm{v}\frac{\partial w}{\partial y} + \mathrm{w}\frac{\partial w}{\partial z} = -\frac{1}{\rho_0}\frac{\partial P}{\partial z} + gz + \frac{\partial}{\partial x}\left(v_x\left(\frac{\partial w}{\partial x} + \frac{\partial u}{\partial z}\right)\right) + \frac{\partial}{\partial y}\left(\mathrm{v_y}\left(\frac{\partial \mathrm{w}}{\partial y} + \frac{\partial \mathrm{v}}{\partial z}\right)\right) + 2\frac{\partial}{\partial z}\left(\mathrm{v_z}\frac{\partial \mathrm{w}}{\partial z}\right) \quad (4)$$

Simulation of tides and currents was carried out by solving the 2D shallow water equations for mass and momentum from the hydrodynamic component of MIKE 21. To solve the 2D shallow water equations using finite difference numerical methods, unstructured numerical grids were used to define the study area bathymetry. The governing wave equation of MIKE 21 is the spectral action balance equation, which for Cartesian coordinates is:

$$\frac{\partial}{\partial t}N + \frac{\partial}{\partial x}C_{g,x}N + \frac{\partial}{\partial y}C_{g,y}N + \frac{\partial}{\partial \sigma}C_{g,\sigma}N + \frac{\partial}{\partial \theta}C_{g,\theta}N = \frac{S}{\sigma} \quad (5)$$

where σ is the relative frequency, θ is wave direction, N is wave action density, which is equal to the energy density divided by the relative frequency (N (σ, θ) = E (σ, θ) / σ) and C_g is the propagation velocity of wave action in (x, y, σ, θ) space. The model is described in the MIKE 21 Wave Modeling Manual, [40]. The last term on the left side of the equation denotes the effects of refraction and shoaling. The source term on the right side is defined as follows:

$$\mathrm{S} = \mathrm{S}_{in} + \mathrm{S}_{nl} + \mathrm{S}_{dis} + \mathrm{S}_{ot} + \mathrm{S}_{surf} \quad (6)$$

where S_{in} represents energy transfer from wind to the waves, S_{nl} is the energy transfer from one frequency to another by nonlinear wave-wave interactions, S_{dis} is wave energy dissipation due to white-capping, S_{ot} is wave power dissipation due to bottom friction, and S_{surf} represents wave power dissipation resulting from wave breaking in shallow waters.

3.2. Oil spill model

The oil spill module uses a random walk model to solve the Fokker-Planck equation for the irregular motion of particles suspended in a fluid (a liquid or gas) resulting from their collision with the fast-moving molecules in the fluid (Deigaard and Hansen, [41]).

In this process, physical and chemical processes affect the motion of each particle. The path and mass of the released particle in the water column are tracked, based on a constant reference frame and in terms of time. The Fokker-Planck equation for suspended oil particles is solved by the Lagrangian decomposition method. In this module, processes that affect the degradation of spilt oil are also investigated. These processes include evaporation, emulsion and penetration in the water column. For more information see MIKE3 Spill Model, [42].

3.3. Data Collection

The topographic data is taken from GEBCO (https://www.gebco.net). The GEBCO grid is a continuous terrain model for ocean and land with a spatial resolution of 30 arc seconds. Wind data, sea level pressure, and air and water temperatures were extracted from ECMWF analysis data, denoted ERA-Interim (https://www.ecmwf.int/en/forecasts) which is available from Jan 1979 to the present, with 0.125° spatial and 6-hour temporal resolutions. The wind speed and air temperature are extracted for 10- and 2-meters reference heights above sea level, respectively.

In the coarse grid, large-scale model implementation, the boundary conditions of the water level are extracted from the Tide Model Driver (TMD) toolbox. Boundary conditions of the local model were also derived from the large-scale model, for water level and flow speed. In addition, the first-order spatial and temporal upwind method was used to solve the advection equations. The density was assumed barotropic and the Coriolis force was applied to the model as a

dependent variable of location. Large- and local-scale models used three- and two-dimensional models, respectively.

According to the International Tanker Owners Pollution Federations (ITOPF) in 2002, oil types are divided into four groups based on density. The oil in this study is the so-called Mississippi Canyon (MC) crude oil with API = 2.35 and density of 0.849 gr/cm^3 (Deep water Horizon MC 252 Response Unified Area Command, 2010). According to the Danish Hydraulic Institute, this oil is part of a group of oil types for which 70% is composed of lightweight component and the remaining 30% is heavyweight oil, of which 7% is wax and 0.6% is asphaltenes. Using this information, the masses of lightweight oil, wax, asphaltenes and the remaining heavyweight oil are approximated as 700, 70, 0.006, and 229.9944, respectively, in terms of kilograms per thousand kilograms (MIKE3 Spill Model, [42]).

A large scale model on the scale of the Gulf with the eastern longitude from -81° to -98° and the northern latitude from 18° to 31° was deployed. The large scale and regional computational grid are compiled using unstructured triangulated meshes. Taking into account the objectives of this study, this gridding provides a suitable grid for hydrodynamic simulation and ensures sufficient accuracy to generate the required information (Goharnejad et. al, [43]; Goharnejad et. al, [44]).

In order to analyze the sensitivity of the computational grid, several grids with different dimensions were used and finally an optimal computational grid was selected for the large- and local- scale models. The final resulting interpolation of bathymetry data and the computational grid used for the large- and local-scale models are presented in Fig. 2.

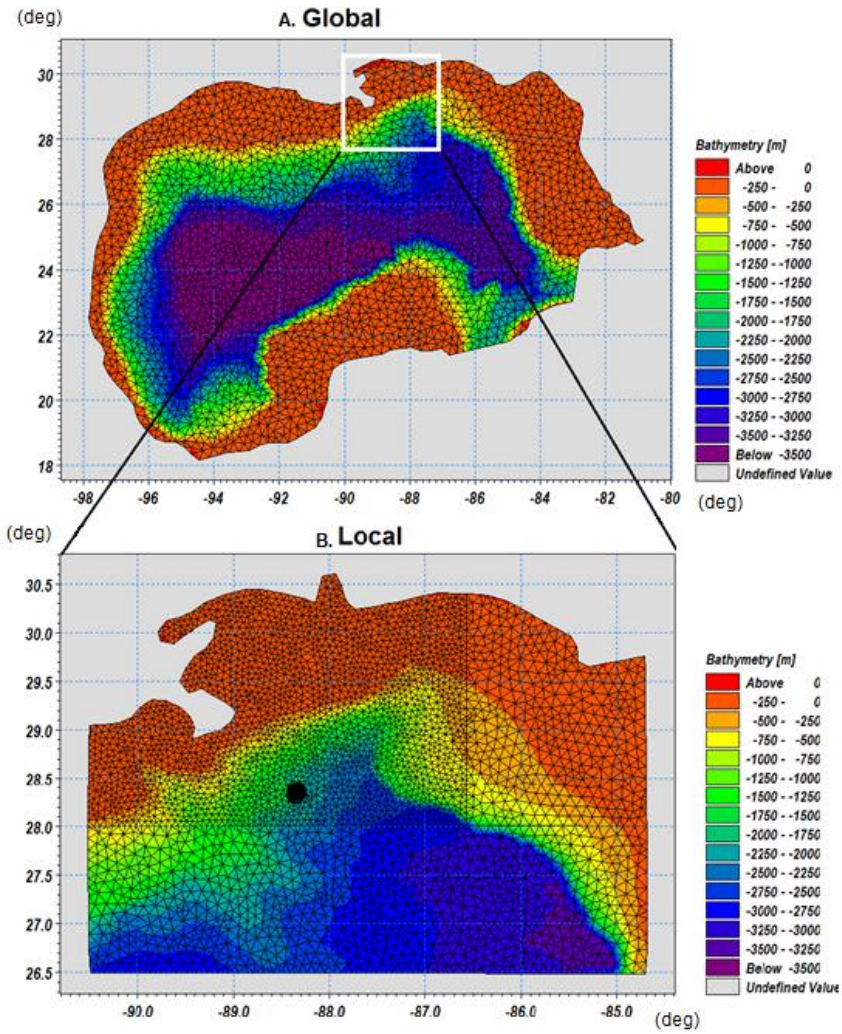

Figure 2. A: large-scale grid and B: local-scale grid models with triangular meshes in the study area

3.4. Observed data

Buoy data extracted from the NDBC website are the main source of observed data. These are used for calibration and validation. Water level measurements are provided by the ioc-sea level monitoring database (www.ioc-sealevelmonitoring.org). Characteristics of these stations are presented in Table 1.

Table 1. Specifications for the buoys used to evaluate the performance of the model

Station ID	Location	Type of device	Water depth (m)	Latitude	Longitude
TG1	Dauphin Island, AL	Tidal Gage	---	30°15'1" N	88°4'30" W
TG2	Grand Isle, LA	Tidal Gage	---	29°15'53" N	89°57'27" W
Buoy 42040	South of Dauphin Island, AL	Wave Gage	183	29°12'30" N	88°13'33" W

3.5. Sensitivity analysis and calibration of the numerical model

In order to evaluate the model performance, statistical parameters for the observed and modeled data were calculated as follows:

- Bias $\text{Bias}=(\bar{S}-\bar{O})$
- Root mean squared errors $\text{RMSE}=\sqrt{\frac{1}{N}\sum(S_i-O_i)^2}$
- Correlation coefficient $\text{CC}=\frac{\sum(S_i-\bar{S})(O_i-\bar{O})}{\sqrt{\sum(S_i-\bar{S})^2\sum(O_i-\bar{O})^2}}$
- dispersion coefficient $\text{SI}=\frac{\sqrt{\frac{1}{N}\sum(S_i-O_i)^2}}{\bar{O}}$

where O_i is the observed value at the i^{th} time step, S_i is a forecast value at the same time step, N is the number of time steps and $\bar{O}$ and $\bar{S}$ is the mean values, of the data, respectively (Goharnejad et al., 2013 [45]).

4. Results

In this section, results of flow model, spectral wave model, and oil spill model are presented. Initially, a verification process was performed to evaluate the performance of the models. For this purpose, the model system was implemented for one-year (2009-2010) and results were compared with the observed buoy data. This process led to an adjustment in the model results for those periods which increased the consistency of the results compared to observed values in other periods. Results are presented in terms of plots and statistical parameters including bias, root mean square error (RMSE), correlation coefficient (CC) and scatter index (SI). Simulation parameters and calibration coefficients for the small (local) scale model are constructed, as for the large-scale model. Results for the observation buoy locations are presented in Fig. 3.

4.1. Evaluation of performance of wind-wave model

In this section, the accuracy of the wind-wave model was examined by comparing the results of the model and the observed buoy data [https://www.ndbc.noaa.gov/]. For this purpose, the observed and modelled values for significant wave heights and wave periods were compared from April to June 2010. The reason for comparison of the data during this period is that the oil spill occurred during this time. In Fig. 4, the time series of the values of the recorded significant wave heights and wave periods derived from the model and the buoy are compared. Statistical parameters related to the significant wave heights and wave periods are presented in Table 2. The results indicate a high degree of consistency between the model results and the buoy measurements.

Table 2. Statistical parameters of wave model performance from April to June 2010

Parameter	Significant Wave Height (Hs(m))	Wave Period (Tp(s))
Bias	-0.13	**0.28**
CC	0.93	**0.80**
RMSE	0.24	**0.26**
SI	0.31	**0.20**

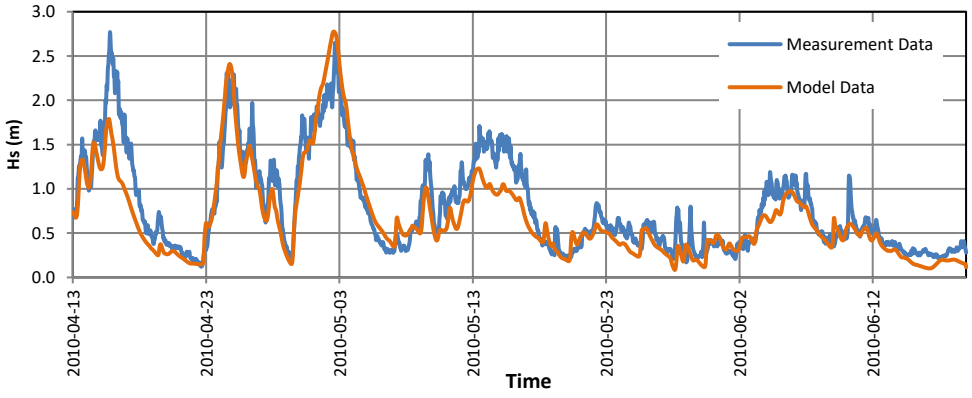

Figure 3. observed and modeled significant wave height time series from April to June 2010

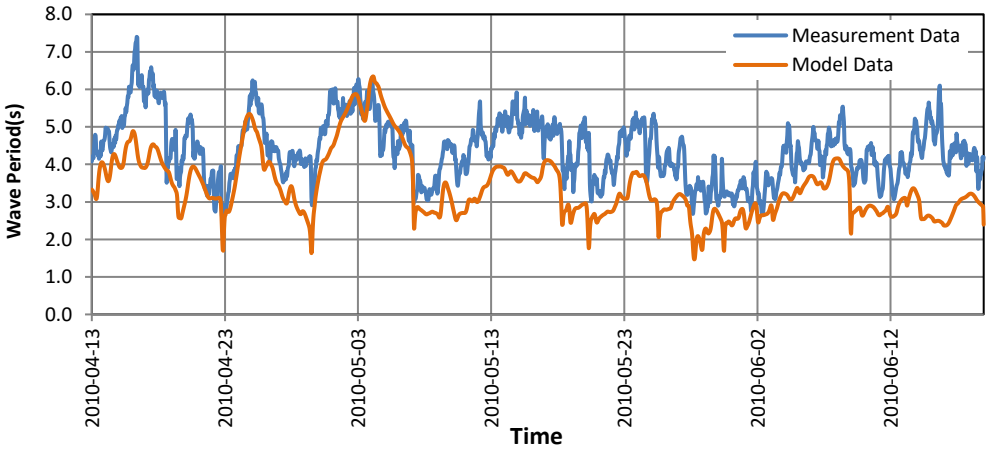

Figure 4. observed and modeled wave period time series from April to June 2010

Critical parameters the spectral wave model include wave breaking, bottom friction, as well as white-capping coefficients. Results suggest that there is high consistency between the model results and observed buoy data. The calibrated parameters used in the spectral wave model are presented in Table 3.

Table 3. Values of parameters used in the numerical model during final calibration of wave model.

Parameter	**Appropriate Value**	
Wave breaking coefficient	Gamma	Alpha
	1.0	0.8
Bottom friction (Nikuradise)coefficient	0.01	
White capping coefficient	C_{dis}	$Delta_{dis}$
	4.5	0.5

4.2. Evaluation of tidal model performance

In order to verify the tidal model in terms of meter, a comparison was made with observed data at two stations, in Figures 5 and 6. Statistical parameters related to model performance are presented in Table 4. The results indicate that water level changes due to tidal effects are consistent with the measured data. There are no significant differences in terms of phases and amplitudes.

Table 4. Statistical parameters of current model performance from April to June 2010.

Station Parameter	TG1-Dauphin Island, AL	TG2- Grand Isle, LA
Bias	0.02	0.01
CC	0.15	0.27
RMSE	0.19	0.19
SI	0.80	0.75

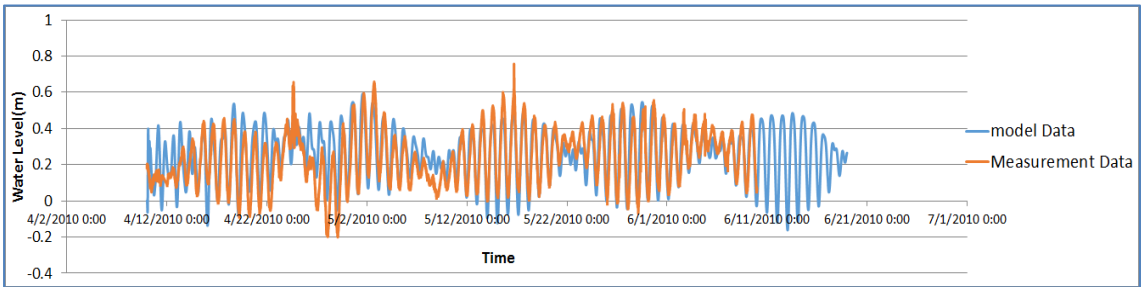

Figure 5. Comparison of water level modeling and TG1-Dauphin Island, AL station records

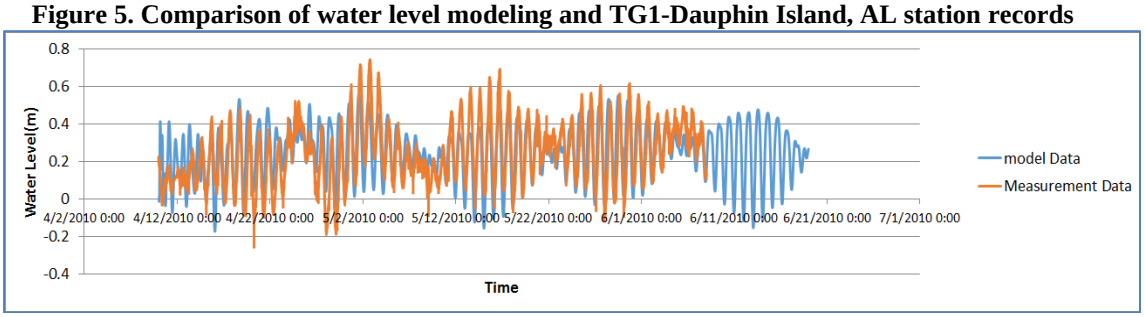

Figure 6. Comparison of water level modeling and TG2-Grand Isle LA station records.

Based on sensitivity analysis, bed resistance and horizontal viscosity coefficient in the flow model exhibit high sensitivity compared to other parameters. Therefore, optimal values for these items are used in calibration of the model. In this methodology, appropriate values of bed resistance and horizontal viscosity coefficients were determined by a sensitivity analysis of differing values; the calibrated values are shown in Table 5.

Table 5. Values of parameters used in MIKE 21 in the final calibration of the hydrodynamic model.

Parameter	Appropriate Value
Bed resistance coefficient	0.01
Horizontal viscosity coefficient	0.28

4.3. Results for spectral wave model and tidal model

Since wind is the main factor in generating and forming waves, wind rose diagrams in winter, spring, summer, autumn, and annual period were constructed at the DWH location as shown in Fig. 7. During winter, the dominant wind blows from the north, while in the spring, the dominant wind blows from the south-east direction, tending toward the east in summer and autumn. Comparison of regional wind rose diagrams show that if the oil spill occurred in autumn or winter, the direction of the oil spill movement would be different.

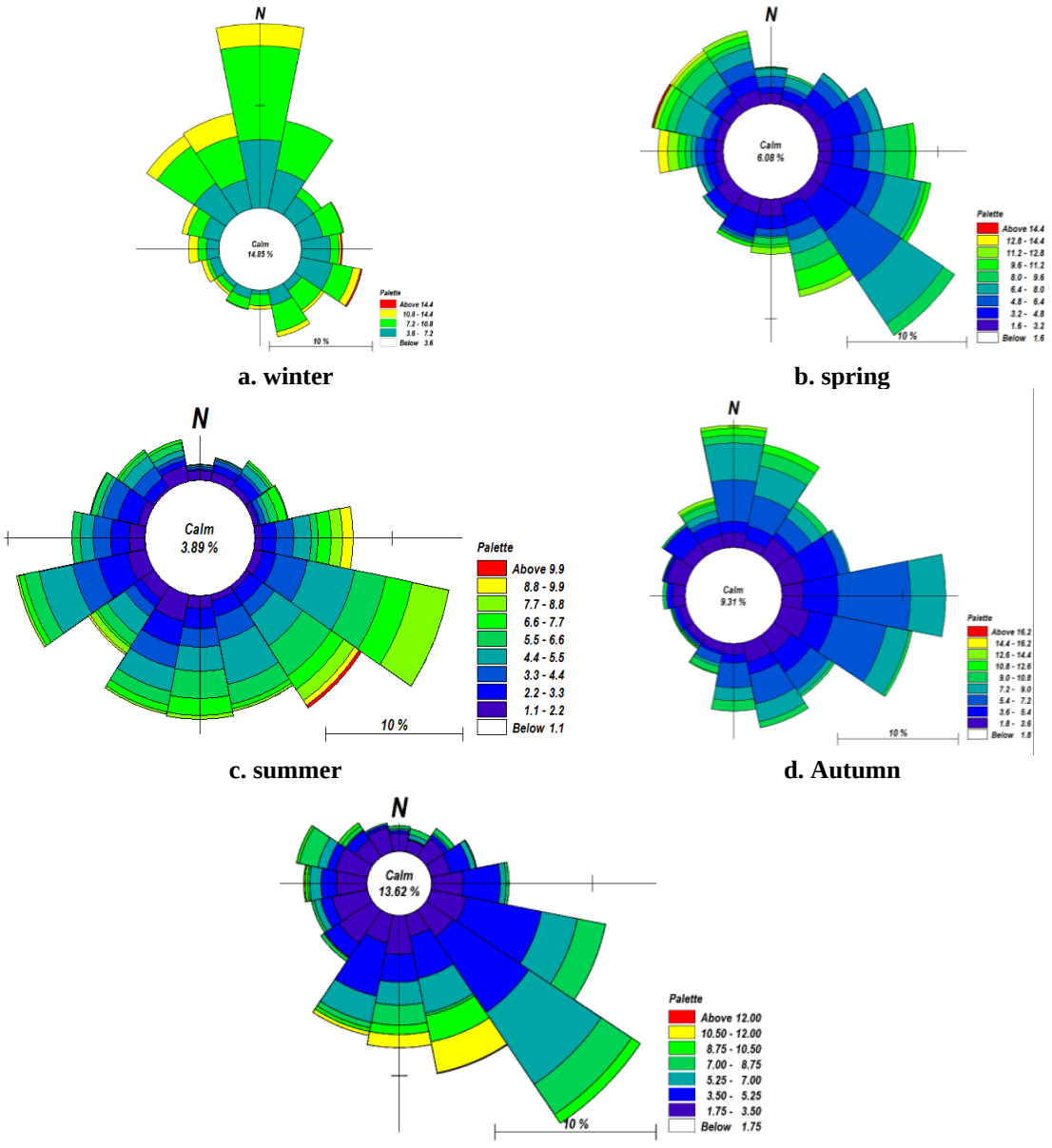

Figure 7.Wind rose diagram at the DWH location in winter, spring, summer, autumn, and annually.

In order to study the wind-wave regimes in this area, the wave roses in each season over an annual period are drawn in Figure 8. The results of wind-wave model show that significant wave heights reach more than 2 meters. However, with the propagation of offshore waves to the coastal areas, relatively large changes in the directions of waves can occur. For this offshore area, the significant wave heights are less than 0.36 m, for 34% of the year, with prevailing wind directions from the southeast. Moreover, based on the statistics of the station and taking into account the total data recorded, in 34% of the year, the wind speed is less than 1.75 m/s.

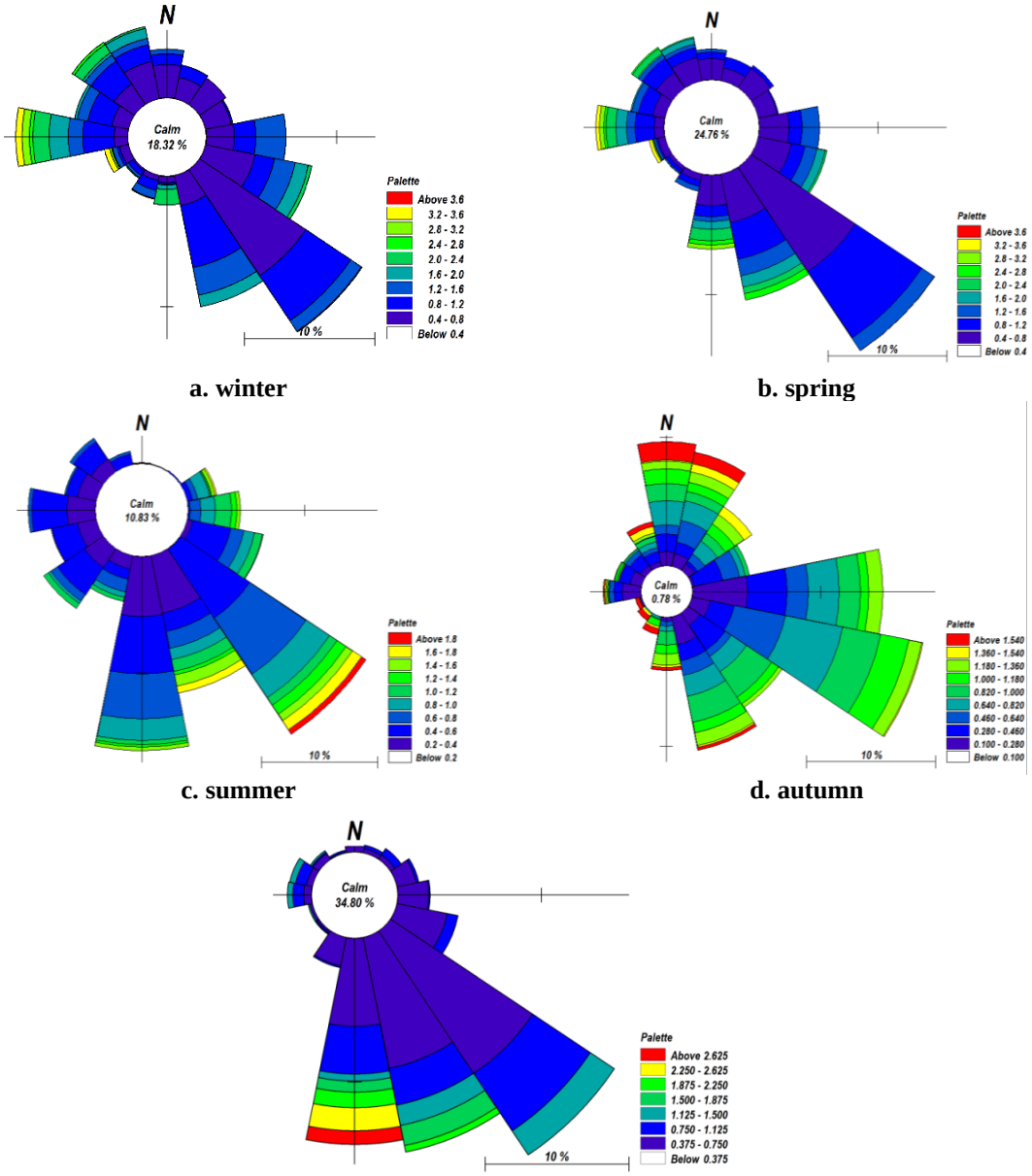

Figure 8. Wave rose at DWH in different seasons (winter, spring, summer, autumn, and annually).

In case of the tidal model, results indicate larger increases in water level and current speed in coastal areas than in deep waters. The most important factor in such variation is the effect of wind shear stress, which is more effective in shallow waters. Therefore, transport of oil contamination in these areas is more rapid. Also, near the Mississippi river delta, vortices appear to be relatively predictable due to the geometry of the area. These vortices have an effect in transferring the contaminants from deeper to shallower areas. Therefore, for the modeling of spilt oil, vortex impacts should be considered. According to flow model results, the maximum sea level and flow speed in the study area are 0.8 m and 0.7 m/s, respectively. Meanwhile, the

annual wave rose diagram shows that the prevailing direction of waves in the oil spill area is southward.

4.4. Results of oil spill model

In order to validate the oil spill model, the motion of the spilt oil is compared to satellite images. Several satellites images are available to cover the DWH oil in the Gulf. In fact, NASA satellite images provided detailed coverage. These satellite images of the Gulf are presented in Fig. 9. These images are taken by the NASA's Terra and Aqua high resolution MODIS (or Moderate Resolution Imaging Spectroradiometer) satellite.

Comparisons of the results of the oil spill model and the satellite images in four different periods of the DWH event are presented in Fig. 9. Results of the oil spill model are shown to be consistent with the satellite images. These indicate that the oil slick spreads, disperses into various different sub-areas, and appears to dissipate and decay. The oil contamination first moved to the north and south and then spread to the west and southwest, plunging to the coast of Louisiana and returning to the sea again. The latitudes and longitudes during the spreading period range from 26.5° to 30° to the north and from 89.5° to 87° to the east.

As a progression in time, by April 25 the length of the oil spill reached 55 kilometers and covered an area of 2,800 square kilometers. By May 9, the oil spill had apparently divided into two slicks, each with an area of about 2420 and 960 square kilometers, respectively. Eventually, by May 28, the slick area appeared to reach over 48,400 square kilometers. It is noteworthy that ultimately, much of the oil evaporated because it was lightweight oil.

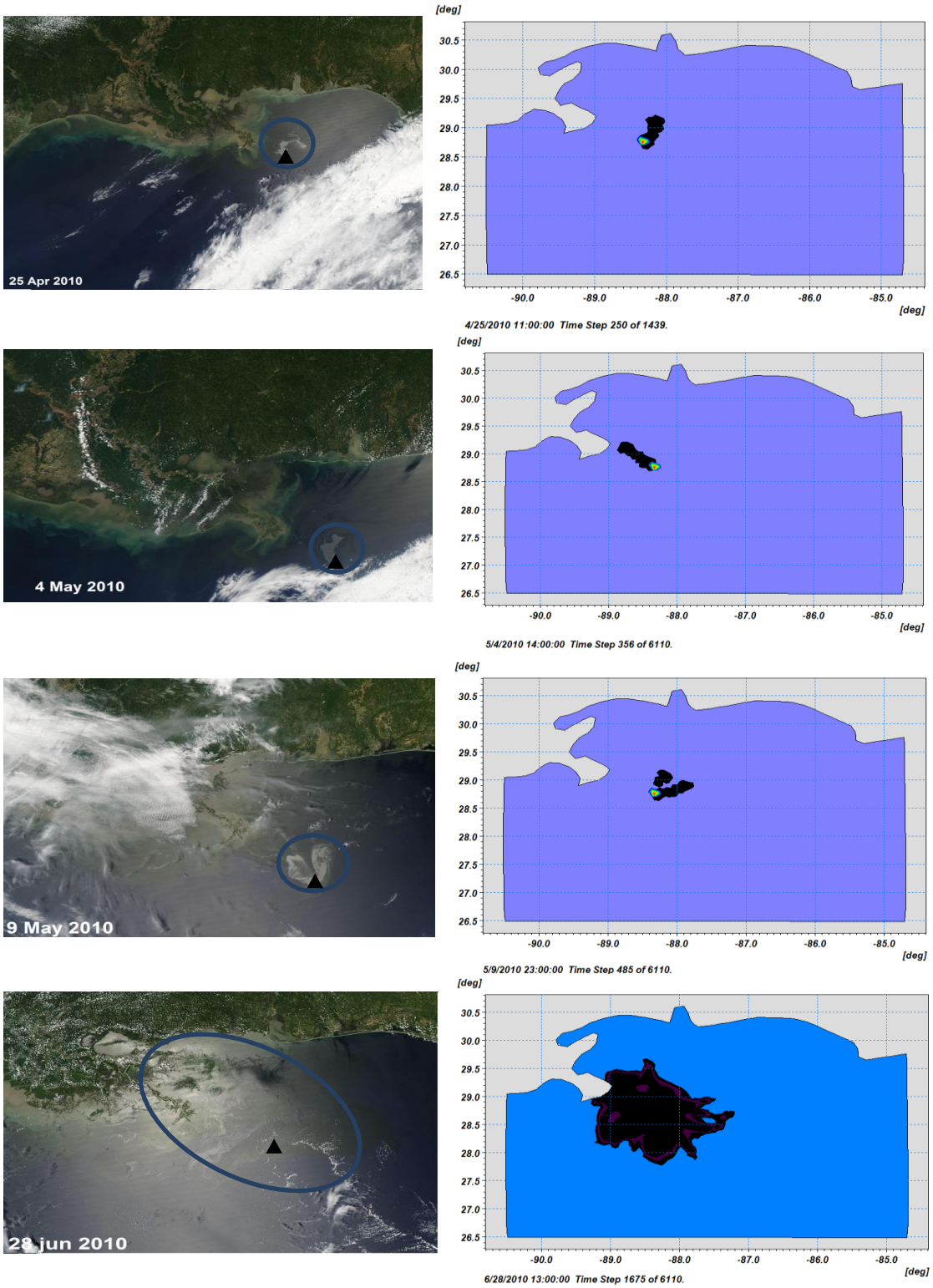

Figure 9. Comparison of DWH oil spill model results to satellite data on April 25, May 4 and 9, and June 28, 1 cm on the map is 50 km in the field.

In terms of fluid dynamics, a vortex is a region in a fluid in which the flow revolves around an axis line, which may be straight or curved (Kida et al, [46]). Hence, the study of horizontal vortices is important in this study because the Mississippi river impacts on the formation of vortex flows, which are effective in the diffusion and transport of contaminations, tracer particles and sediments.

One of the important features of horizontal vortices is the significant reduction in the flow velocity at the center of the vortex, which causes the deposition of pollutants. Figure 10 depicts vortex patterns around the oil spill area and consequent oil dispersion.

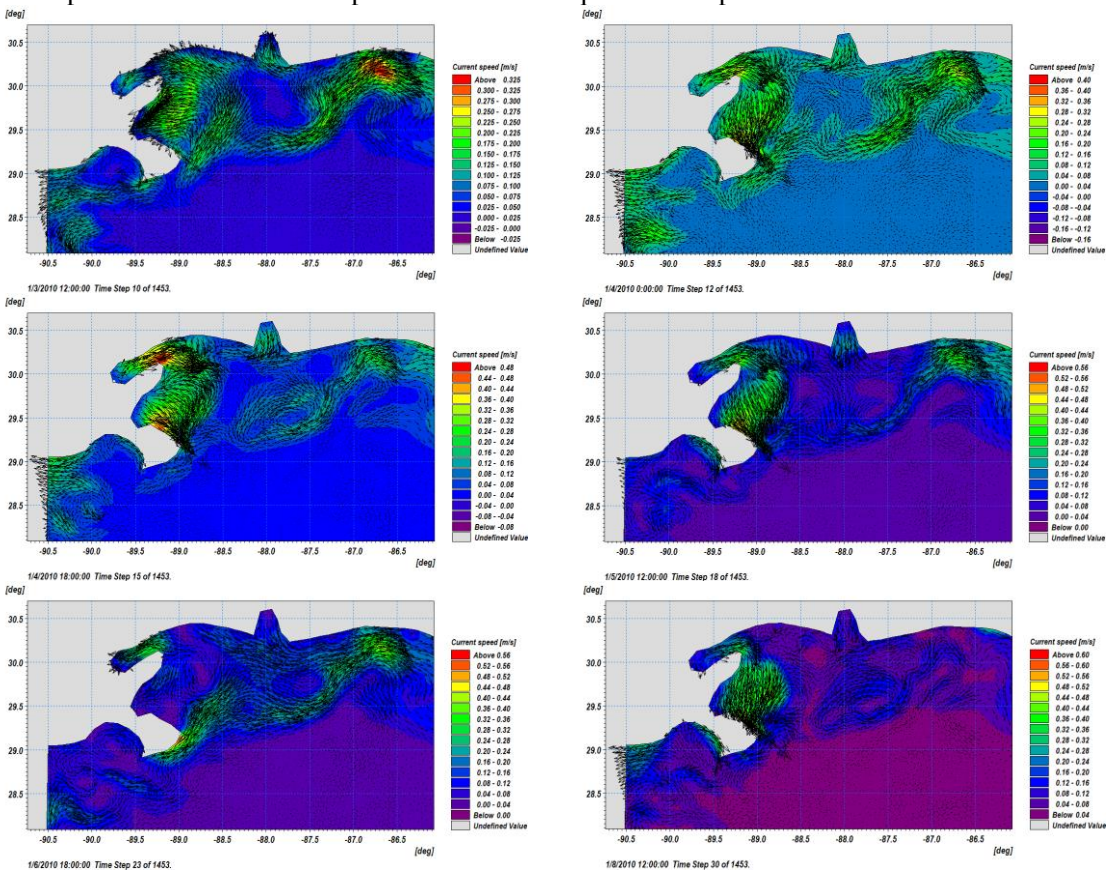

Figure 10. Horizontal vortices in the study area.

4.5. Seasonal Variations

Regarding the fact that the hydrodynamic behavior of the Gulf of Mexico changes in different seasons due to variations in atmospheric regimes, two different scenarios are considered in this study. These are motivated by possible scenarios whereby the oil spill might occur in other seasons; what would be the oil spill trajectory? The model simulations were computed in two winter seasons and two autumn seasons to provide overall oil spill patterns in these two seasons. With regard to possible oil spills in the spring and summer, the modelled oil spill results are similar to results in the two winters and two autumns. After 17 days, the overall dispersion and transport of spilt oil in these two seasons are presented in Figures 11 and 12. These two figures suggest southward motion of the spilt oil (along the directions of wind and current). Moreover, the oil spill sizes are approximately similar in these two examples.

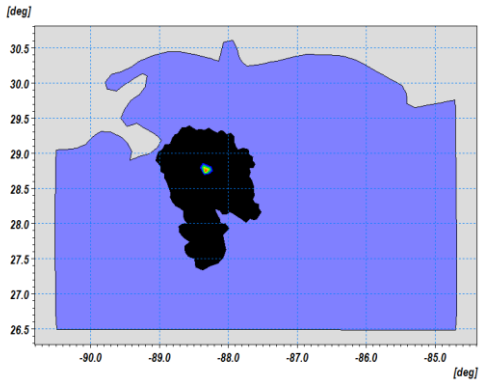

Figure 11. Hypothetical position of oil spill particles during Autumn 2010

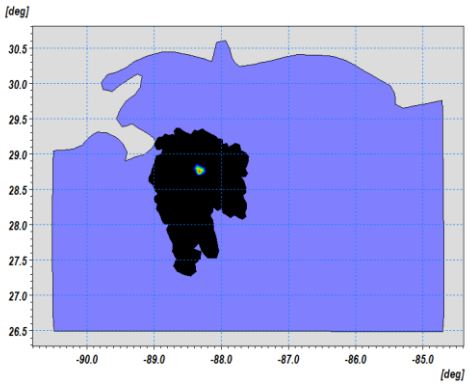

Figure 12. Hypothetical position of oil spill particles during winter time 2010

5. Conclusion

The purpose of this study is to study oil spill phenomena, considering two scenarios using the numerical model, MIKE21. Initially, the hydrodynamic conditions of the Gulf of Mexico were modeled and the appropriate parameters were calibrated. Based on wind and wave rose diagrams at the DWH site of the spill, the prevailing directions of waves and currents were westerlies and the wind predominantly blew from the southeast.

The results of the oil spill model are demonstrated as a series of two-dimensional images from April 25 to June 28, 2010. During this time, the massive oil spill evolved into smaller oil spills, spreading over the ocean, and decaying. Considering the dominant wave and current directions, it can be concluded that the influence of the currents and the waves has more effect than the wind in displacement of the spilt oil. According to results and in comparison, with other studies (Wan and Cheng, [24]), our provided results are highly consistent with these studies.

Meanwhile, a calculation of the expected oil spill trajectories in autumn and winter also indicates that the oil spill motions in these two seasons are southward (along with the dominant directions of the wind and flow), and the extent of the oil spill size is approximately the same in either season. Atmospheric factors are the most important determinants in the formation of sea levels, flow speed, and waves and also appear to be of utmost importance in the dispersion and transport of oil spills. The projections presented in this study are extracted by numerical modeling. Clearly the concomitant errors caused by numerical modeling may have significant effects on the results. Nevertheless, validation of results of the models has been verified in quantitative and qualitative terms. Therefore, the present study suggests that the MIKE numerical model is relatively accurate in modelling the hydrodynamics, waves, and dispersion and transport of spilt oil in the Gulf.

References

1. Raoufi, S.S., Goharnejad, H. and Niri, M.Z., 2018. Air pollution effects on climate and air temperature of Tehran city using remote sensing data. Asian Journal of Water, Environment and Pollution, 15(2), pp.79-87.
2. Asadi, A., Goharnejad, H. and Niri, M.Z., 2019. Regression modelling of air quality based on meteorological parameters and satellite data. Journal of Elementology, 24(1).

3. ASCE Task Committee on Modeling of Oil Spills, 1996. State-of-the-art review of modeling transport and fate of oil spills. Journal of Hydraulic Engineering, 122(11), pp.594-609.
4. Javid, A., 2002. Three dimensional modeling of contaminants transportation (oil spill) in Caspian Sea (Doctoral dissertation, Islamic Azad University, Science and Research Branch, Tehran).
5. Armanfar, M., Goharnejad, H., Niri, M.Z. and Perrie, W., 2019. Assessment of coastal vulnerability in Chabahar Bay due to climate change scenarios. Oceanologia, 61(4), pp.412-426.
6. Goharnejad, H. and Eghbali, A.H., 2015. Forecasting the Sea Level Change in Strait of Hormuz. World Acad Sci Eng. Technol Int J Environ Chem Ecol Geol Geophys Eng, 9, pp.1319-1322.
7. Fay, J.A., 1969. The spread of oil slicks on a calm sea. In Oil on the Sea (pp. 53-63). Springer, Boston, MA.
8. Fay, J.A., 1971, June. Physical processes in the spread of oil on a water surface. In International Oil Spill Conference (Vol. 1971, No. 1, pp. 463-467). American Petroleum Institute.
9. Stolzenbach, K.D., Madsen, O.S., Adams, E.E., Pollack, A.M. and Cooper, C., 1977. A review and evaluation of basic techniques for predicting the behavior of surface oil slicks.
10. Lehr, W.J., Cekrige, H.M, Fraga, R.J., Belen, M.S., 1984. Emprical studies of the spreading of oil spills. Oil and Petrochemical Pollution 2,7-11.
11. Elliott, A.J., 1986. Shear diffusion and the spread of oil in the surface layers of the North Sea. Deutsche Hydrografische Zeitschrift, 39(3), pp.113-137.
12. Weber, J.E., 1983. Steady wind-and wave-induced currents in the open ocean. Journal of Physical Oceanography, 13(3), pp.524-530.
13. Jenkins, A.D., 1986. A theory for steady and variable wind-and wave-induced currents. Journal of Physical Oceanography, 16(8), pp.1370-1377.
14. Al-Rabeh, A.H., Cekirge, H.M. and Gunay, N., 1989. A stochastic simulation model of oil spill fate and transport. Applied Mathematical Modelling, 13(6), pp.322-329.
15. Fingas, M. and Fieldhouse, B., 2003. Studies of the formation process of water-in-oil emulsions. Marine pollution bulletin, 47(9-12), pp.369-396.
16. Owens, E.H., Taylor, E. and Humphrey, B., 2008. The persistence and character of stranded oil on coarse-sediment beaches. Marine pollution bulletin, 56(1), pp.14-26.
17. Mariano, A.J., Kourafalou, V.H., Srinivasan, A., Kang, H., Halliwell, G.R., Ryan, E.H. and Roffer, M., 2011. On the modeling of the 2010 Gulf of Mexico oil spill. Dynamics of Atmospheres and Oceans, 52(1-2), pp.322-340.
18. North, E.W., Adams, E.E., Schlag, Z., Sherwood, C.R., He, R., Hyun, K.H. and Socolofsky, S.A., 2011. Simulating oil droplet dispersal from the Deepwater Horizon spill with a Lagrangian approach. Geophys. Monogr. Ser, 195, pp.217-226.
19. Zhang, X., Marta-Almeida, M. and Hetland, R.D., 2012. A high-resolution pre-operational forecast model of circulation on the Texas-Louisiana continental shelf and slope. Journal of Operational Oceanography, 5(1), pp.19-34.

20. Marques, W.C., Stringari, C.E., Kirinus, E.P., Möller Jr, O.O., Toldo Jr, E.E. and Andrade, M.M., 2017. Numerical modeling of the Tramandaí beach oil spill, Brazil—Case study for January 2012 event. Applied Ocean Research, 65, pp.178-191.
21. French-McCay, D.P., Spaulding, M.L., Crowley, D., Mendelsohn, D., Fontenault, J. and Horn, M., 2021. Validation of Oil Trajectory and Fate Modeling of the Deepwater Horizon Oil Spill. Frontiers in Marine Science, 8, p.136.
22. Tri, D.Q., Don, N.C. and Ching, C.Y., 2013. Trajectory modeling of marine oil spills: case study of Lach Huyen port, Vietnam. Lowland Technology International, 15, pp.41-55.
23. Pisano, A., Bignami, F. and Santoleri, R., 2015. Oil spill detection in glint-contaminated near-infrared MODIS imagery. Remote Sensing, 7(1), pp.1112-1134.
24. Wan, J. and Cheng, Y., 2013, June. Remote sensing monitoring of Gulf of Mexico oil spill using ENVISAT ASAR images. In 2013 21st International Conference on Geoinformatics (pp. 1-5). IEEE.
25. Caruso, M.J., Migliaccio, M., Hargrove, J.T., Garcia-Pineda, O. and Graber, H.C., 2013. Oil spills and slicks imaged by synthetic aperture radar. Oceanography, 26(2), pp.112-123.
26. Sun, S., Hu, C., Feng, L., Swayze, G.A., Holmes, J., Graettinger, G., MacDonald, I., Garcia, O. and Leifer, I., 2016. Oil slick morphology derived from AVIRIS measurements of the Deepwater Horizon oil spill: Implications for spatial resolution requirements of remote sensors. Marine pollution bulletin, 103(1-2), pp.276-285.
27. Khade, V., Kurian, J., Chang, P., Szunyogh, I., Thyng, K. and Montuoro, R., 2017. Oceanic ensemble forecasting in the Gulf of Mexico: An application to the case of the Deep Water Horizon oil spill. Ocean Modelling, 113, pp.171-184.
28. White, H.K., Conmy, R.N., MacDonald, I.R. and Reddy, C.M., 2016. Methods of oil detection in response to the Deepwater Horizon oil spill. Oceanography, 29(3), pp.76-87.
29. Deis, D.R., Mendelssohn, I.A., Fleeger, J.W., Bourgoin, S.M. and Lin, Q., 2019. Legacy effects of Hurricane Katrina influenced marsh shoreline erosion following the Deepwater Horizon oil spill. Science of The Total Environment, 672, pp.456-467.
30. Garcia-Pineda, O., Macdonald, I., Hu, C., Svejkovsky, J., Hess, M., Dukhovskoy, D. and Morey, S.L., 2013. Detection of floating oil anomalies from the Deepwater Horizon oil spill with synthetic aperture radar. Oceanography, 26(2), pp.124-137.
31. Lončar, G., Leder, N. and Paladin, M., 2012. Numerical modelling of an oil spill in the northern Adriatic. Oceanologia, 54(2), pp.143-173.
32. Badri, MA, Faghihi Fard, M., 2015, Numerical Simulation of Oil Pollution Due to Turbulence Flow Pattern, Wind and Tide Effects, Mechanical Engineering Journal, 73 (4), Pp. 15-22 (In Persian)
33. Appendini, C.M., Torres-Freyermuth, A., Salles, P., López-González, J. and Mendoza, E.T., 2014. Wave climate and trends for the Gulf of Mexico: A 30-yr wave hindcast. Journal of Climate, 27(4), pp.1619-1632.
34. Xue, Z., Zambon, J., Yao, Z., Liu, Y. and He, R., 2015. An integrated ocean circulation, wave, atmosphere, and marine ecosystem prediction system for the South Atlantic Bight and Gulf of Mexico. Journal of Operational Oceanography, 8(1), pp.80-91.

35. Huang, Y., Weisberg, R.H., Zheng, L. and Zijlema, M., 2013. Gulf of Mexico hurricane wave simulations using SWAN: Bulk formula-based drag coefficient sensitivity for Hurricane Ike. Journal of Geophysical Research: Oceans, 118(8), pp.3916-3938.
36. Huerta, A.D. and Harry, D.L., 2012. Wilson cycles, tectonic inheritance, and rifting of the North American Gulf of Mexico continental margin. Geosphere, 8(2), pp.374-385.
37. McNutt, M., Camilli, R., Guthrie, G., Hsieh, P., Labson, V., Lehr, B., Maclay, D., Ratzel, A., Sogge, M., 2011. Assessment of flow rate estimates for the Deepwater Horizon/Macondo Well Oil Spill. Flow Rate Technical Group report to the National Incident Command, Interagency Solutions Group, March 10, 2011.
38. Deep water Horizon MC 252 Response Unified Area Command, 2010. Strategic Plan for Sub-Sea and Sub-Surface Oil and Dispersant Detection, Sampling, and Monitoring, November 13.
39. Labson, V.F., Clark, R.N., Swayze, G.A., Hoefen, T.M., Kokaly, R., Livo, K.E., Powers, M.H., Plumlee, G.S., Meeker, G.P., 2010. Estimated Minimum Discharge Rates of the Deepwater Horizon Spill – Interim Report to the Flow Rate Technical Group from the Mass Balance Team. USGS Open-File Report 2010-1132
40. Water, D.H.I., 2003. Environment, MIKE 21 Wave Modelling User Guide. DHI Software.
41. Deigaard, R. and Hansen, E.A., 1994. Simulation of Turbulent Diffusion of Suspended Sediment by a Random Walk Mode. EV.
42. Water, D.H.I., 2012. MIKE3 Spill Model, Spill Analysis Module User Guide. DHI Software.
43. Goharnejad, H., Nikaein, E. and Perrie, W., 2021. Assessment of wave energy in the Persian Gulf: An evaluation of the impacts of climate change. Oceanologia, 63(1), pp.27-39.
44. Goharnejad, H., Shamsai, A., Nazif, S. and Zakeri, N.M., 2019. Pridiction of Sea Level Rise in the South of Iran Coastline: Evaluation of Climate Change Impacts.
45. Goharnejad, H., Shamsai, A. and Hosseini, S.A., 2013. Vulnerability assessment of southern coastal areas of Iran to sea level rise: evaluation of climate change impact. Oceanologia, 55(3), pp.611-637.
46. Kida, S., Goto, S. and Makihara, T., 2002. Life, structure, and dynamical role of vortical motion in turbulence. National Institute for Fusion Science, Theory and Computer Simulation Center, pp.1-2.